Measurement and Parameterization of Carrier Mobility Sum in Silicon as a Function of Doping, Temperature and Injection Level

P. Zheng, F. E. Rougieux, D. Macdonald, and A. Cuevas

***Abstract*—Based on contactless photoconductance measurements of silicon wafers, we have determined the sum of the electron and hole mobilities as a function of doping, excess carrier concentration, and temperature. By separately analyzing those three functional dependences, we then develop a simple mathematical expression to describe the mobility sum as a function of carrier injection wafer doping and temperature from 150 to 450 K. This new parameterization also provides experimental validation to Klaassen's and Dorkel–Leturcq's mobility models in a range of temperatures.**

***Index Terms*—Charge carrier mobility, mobility sum, silicon, temperature and injection dependent.**

I. Introduction

An effective way to determine the recombination parameters of defects in silicon is through temperature and injection dependent measurements of the minority carrier lifetime, together with the Shockley–Read–Hall model for defect-assisted recombination [1]. A convenient implementation of this method is to use a temperature dependent photoconductance measurement setup [2]. However, the conversion of the measured photoconductance into an excess carrier density requires knowledge of the sum of the electron and hole mobilities as a function of temperature, doping, and injection level.

Numerous experimental data on the minority and majority carrier mobility in both *p* and *n*-type silicon over a wide range of temperatures have been published, mostly as a function of the dopant concentration [3]–[8]. However, data for the electron and hole mobility sum as a function of excess carrier density available to date have only been measured at room temperature [9]–[12]. Experimental evidence on the simultaneous impact of excess carrier injection and temperature does not exist, to our knowledge. In this study, we determine the sum of the electron and hole mobilities as a function of both excess carrier density and temperature. Based on the measurements, we then derive a comprehensive empirical model that includes injection, doping, and temperature dependences for the carrier mobility sum and is therefore ideally suited to lifetime spectroscopy of defects in silicon.

Manuscript received October 25, 2013; revised December 1, 2013; accepted December 3, 2013. Date of publication January 2, 2014; date of current version February 17, 2014. This work was supported by the Australian Research Council (ARC) and the Australian Renewable Energy Agency (ARENA) fellowships program.

The authors are with the Research School of Engineering, College of Engineering and Computer Science, The Australian National University, Canberra ACT 0200, Australia (e-mail: peiting.zheng@anu.edu.au; fiacre.rougieux@anu.edu.au; daniel.macdonald@anu.edu.au; andres.cuevas@anu.edu.au).

Color versions of one or more of the figures in this paper are available online at http://ieeexplore.ieee.org.

Digital Object Identifier 10.1109/JPHOTOV.2013.2294755

II. Experimental Methods

The samples used in this study were *n*-type crystalline phosphorous doped silicon wafers. We used three Float zone wafers of resistivity 1.0 Ω.cm, 10 Ω.cm, 100 Ω.cm, and two Czochralski-grown wafers of resistivity 0.5 Ω.cm and 25 Ω.cm. The samples were prepared by damage etching and RCA cleaning, followed by surface passivation at 400 °C with plasma-enhanced chemical vapor-deposited silicon nitride films.

The minority carrier lifetime was measured using a calibrated photoconductance tester from Sinton Instruments. In order to measure the simultaneous temperature and injection dependence of the mobility, we used a purpose-built, temperature-controlled inductive coil photoconductance instrument [2]. The mobility sum is determined by comparing transient photoconductance decay and quasi-steady state photoconductance (QSSPC) measurements of the excess conductance ($\Delta\sigma$) for every sample. More details of the method can be found in [13]. To obtain accurate measurements using this technique, sufficient low surface recombination velocity (SRV) is required to ensure a uniform excess carrier profile. The values of SRV, calculated using the Auger limit from Richter *et al* [14], ranged from 16 to 39 cm.s^{-1} for all samples. Based on the measured SRV, computer simulations in [15] show that the difference in excess carrier density between the front and back surfaces is less than 10% for all the samples, which is sufficient for the measurement. The uncertainty of the mobility sum is estimated by assuming a $\pm 3\%$ uncertainty in the measurement of the generation rate (required for the QSSPC method) and an uncertainty of $\pm 5\%$ in the measurement of the conductance $\Delta\sigma$ [16].

III. Results

Fig. 1(a) shows the mobility sum $\mu_{\rm sum} = \mu_n + \mu_p$ at 30 °C as a function of excess carrier density for the five different dopant concentrations ranging from 4×10^{13} cm^{-3} to 1×10^{16} cm^{-3}. At a given excess carrier density, the mobility sum decreases with the dopant density. This is consistent with the expectation that ionized impurity scattering is higher in the more highly doped samples.

However, as shown in Fig. 1(b), when $\mu_{\rm sum}$ is plotted as a function of the sum of excess carrier density and the ionized dopant concentration (that is, as a function of the total

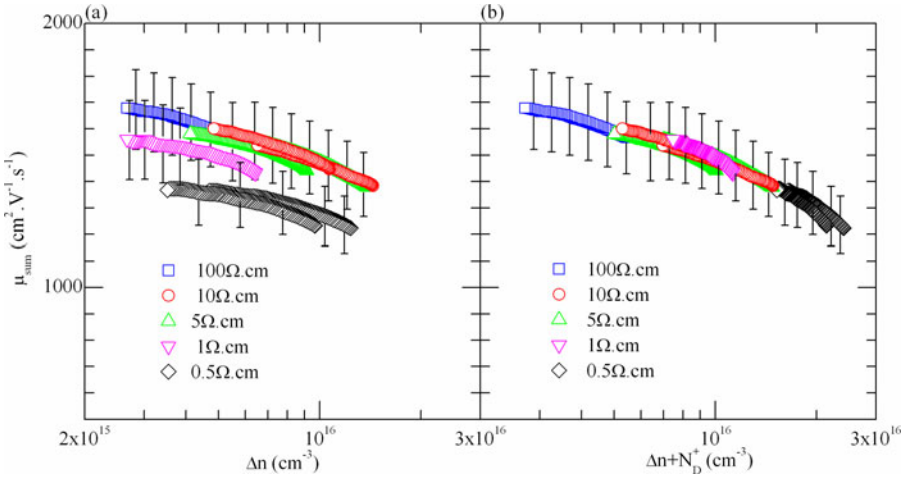

Fig. 1. (a) Measured mobility sum as a function of excess carrier density at 30 °C for five samples of different doping. (b) Measured mobility sum as a function of the sum of excess carrier density and the ionized doping density at 30 °C.

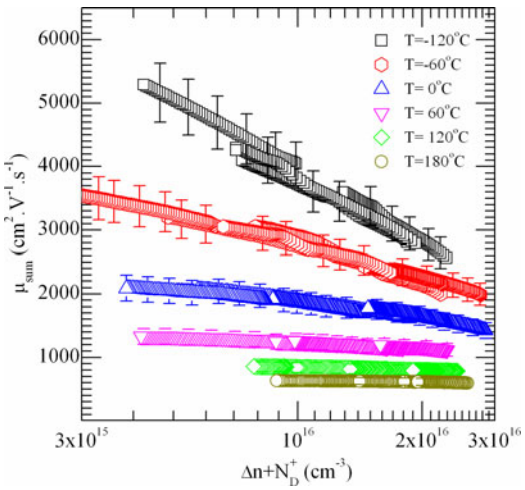

Fig. 2. Measured mobility sum as a function of the sum of excess carrier density and the ionized doping density at −120 °C, −60 °C, 0 °C, 60 °C, 120 °C, and 180 °C.

concentration of majority carriers), the curves for the highly doped samples are shifted to the right and align themselves with the lowly doped samples. This indicates that majority carriers that arise from the dopant atoms have a similar impact on the mobility as excess carriers generated by light. This interesting observation will be discussed in more detail in Section IV.

The measurement results for other temperatures, ranging from −120 °C to 180 °C, are shown in Fig. 2. As above, the mobility sum forms a continuous curve when plotted against the sum of excess carrier density and the ionized dopant concentration. Fig. 2 also shows that increased phonon (lattice) scattering produces a reduction of the mobility as temperature increases. This causes the mobility sum to become less dependent on carrier injection and doping

IV. Empirical Model for the Mobility Sum

From the above experimental results, we can derive an empirical mobility sum model as a function of temperature, ionized dopant density, and carrier injection level.

As a starting point, we adopt the parameterization of $\mu_{\rm sum}$ in the WCT-100 software used in the analysis of QSSPC lifetime measurements [17], [18].This expression is based on Danhauser and Krause's data [9], [10], who measured the mobility sum as a function of carrier injection at room temperature. The expression is

$$\mu_{\rm sum} = \mu_{\rm max} \frac{1 + \left(\frac{N_A + N_D + \Delta n}{N_{\rm ref}}\right)^{\alpha}}{1 + \beta \left(\frac{N_A + N_D + \Delta n}{N_{\rm ref}}\right)^{\alpha}} \tag{1}$$

where N_A is the acceptor concentration, N_D is the donor concentration, Δn is the excess carrier density, $\mu_{\rm max} = 1800$ cm^2·V^{-1}·s^{-1}, $\beta = 8.36$, $\alpha = 0.8431$, and $N_{\rm ref} = 1.2 \times 10^{18}$ cm^{-3}. This simple formula takes carrier density and ionized dopant concentration into account, but it does not include the temperature. The expression can be rearranged as follows:

$$\mu_{\rm sum} = \mu_{\rm max} + \frac{\mu_{\rm min} - \mu_{\rm max}}{1 + \left(\frac{1}{\beta}\right)\left(\frac{N_{\rm ref}}{N_A + N_D + \Delta n}\right)^{\alpha}} \tag{2}$$

where $\mu_{\rm min} = \mu_{\rm max}/\beta$. Equation (2) can be further transformed into the following form:

$$\log\left(\frac{\mu_{\rm sum} - \mu_{\rm min}}{\mu_{\rm max} - \mu_{\rm sum}}\right) = -\alpha \log\left(N_A^- + N_D^+ + \Delta n\right) + \alpha \log\left(N_{\rm ref}\right) + \log\left(\frac{1}{\beta}\right). \tag{3}$$

The mobility in (2) depends on Δn ($\Delta n = \Delta p$) rather than $2 \times \Delta$n. Indeed, only electron-hole scattering reduces the mobility (electron–electron and hole–hole scattering redistribute momentum but does not reduce it). The dopant concentrations in (2) have been replaced by the ionized dopant concentrations for both donors and acceptors [19], [20]. This is essential in our model, since the dopants are not completely ionized at low temperatures, therefore ionized doping density should be used to account for impurity scattering because of Coulombic effects of the ionized dopants. Having both acceptor and donor densities incorporated this way assumes the scattering cross-section

of both donors and acceptors to be similar, which is not always valid [21]. Similarly, having both dopant density and excess carrier density in the same variable assumes that the scattering cross section of two moving particles (an electron and a hole) is the same as the scattering cross section of a static dopant and a moving particle (e.g., donor and hole) which is not always valid in principle [22]. However, such physical considerations were not found to negatively affect the fitting of the experimental data in the injection range covered by this study, as can be observed in Figs. 1 and 2.

We have linearized (2) by taking its logarithm. Hence, in (3), $-\alpha$ is the slope, and $\alpha\log\,(N_{\rm ref}) + \log\,(1/\beta)$ is the intercept of the linear relationship. The parameters $\mu_{\max}$ and β can be optimized by maximizing the correlation coefficient of log $((\mu–\mu_{\min})/(\mu_{\max}–\mu))$ and $\log(N_A^- + N_D^+ + \Delta n)$. The parameters α and $N_{\rm ref}$ are calculated from a least square fit to the experimental data, where α is the slope of the straight line and $N_{\rm ref}$ can be obtained from the intercept.

The model has four fitting parameters as seen in (3), $\mu_{\min}$ depends on both $\mu_{\max}$ and β. Since our experimental data are scarce in the high injection range, there are a number of parameter combinations that can be derived at each temperature. However, two reasonable assumptions can be made to arrive at a unique set of parameters that fit all the experimental data. They are the following:

1) The range of the experimental data available for this mobility model span from $\Delta n + N_D^+ = 3 \times 10^{15}$ cm^{-3} to 3×10^{16} cm^{-3} (see Fig. 2). It is important to note that $\mu_{\min}$ only has a significant impact in the high injection range and has a minor influence on the fitting of the model in the range available. Therefore, we can make a reasonable assumption that $\mu_{\min}$ and $\mu_{\max}$ have the same temperature dependence and are related through the same β at each temperature. The value $\beta = 8.36$ from (1) above is used in the following.
2) With known $\mu_{\max}$ and β, it is found that the slope $(-\alpha)$ of the experimental curve at each temperature lies between -0.95 and -1 and does not show any temperature dependence. Therefore, we assume that α is independent of temperature with an average value of 0.97.

Fig. 3 plots the linearized mobility data used in the fitting of the model. The solid lines are calculated from the right hand side of (3) by adjusting the reference dopant density $(N_{\rm ref})$. The symbols are obtained from the experimental data with $\mu_{\max}$ that gives the best correlation coefficient to the data. An excellent agreement between fit and experimental data is found at every temperature.

As $\mu_{\max}$ is derived from the experimental data at each temperature, all the $\mu_{\max}$ are plotted in Fig. 4 and the temperature dependence can be derived with the well-known power dependence as (see e.g., references [23]–[25])

$$\mu_{\max}(T) = \mu_{\max\,300\rm K}\left(\frac{T}{300}\right)^{\gamma} \tag{4}$$

where $\mu_{\max 300\,\rm K}$ is the maximum mobility sum at 300 K and γ is the power factor to fit the $\mu_{\max}$ curve. The values of $\mu_{\max 300\,\rm K}$ and γ are listed in Table I. The resulting fit is plotted

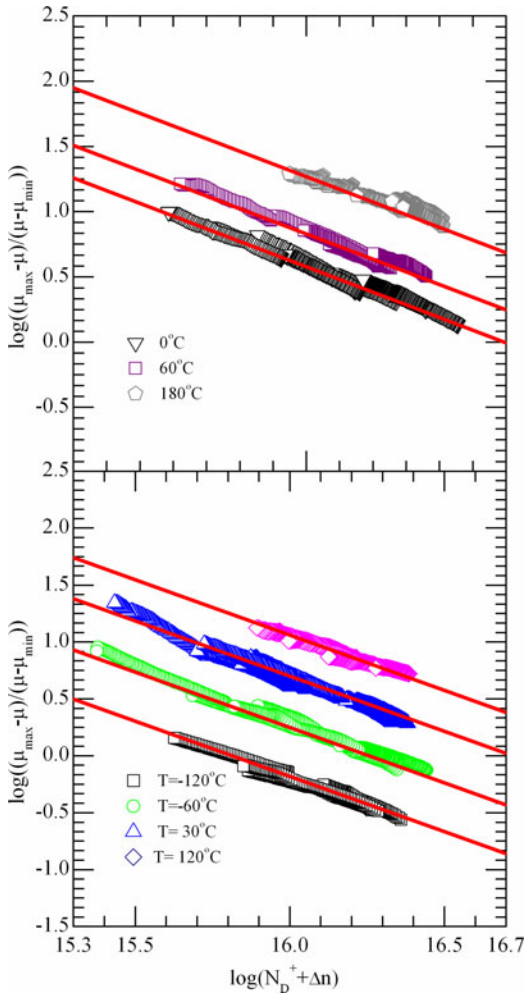

Fig. 3. Fitting of measured mobility sum using (3) at -120 °C, -60 °C, 0 °C, 30 °C, 60 °C, 120 °C, and 180 °C. The symbols are calculated based on the left hand side of (3), the solid lines are the fitting using the right hand side of (3) by adjusting $N_{\rm ref}$ and α.

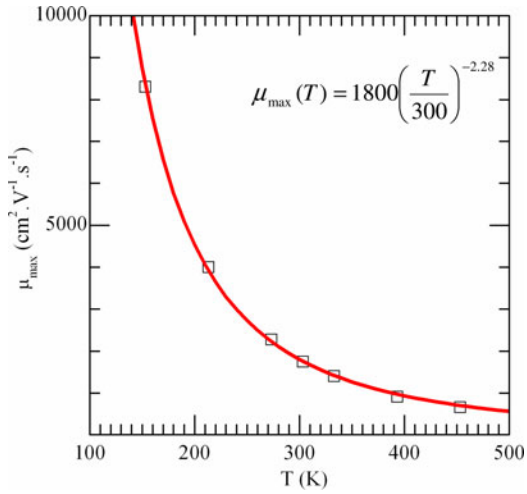

Fig. 4. Temperature dependence of the fitting parameter $\mu_{\max}$. This parameter is extracted from the experimental data and subsequently fitted using (4).

TABLE I
PARAMETERS FOR MOBILITY SUM MODEL

Parameters	
$\mu_{max300K}$	1800 $cm^2 \cdot V^{-1} \cdot s^{-1}$
$N_{ref300K}$	$4.65 \times 10^{17} cm^{-3}$
β	8.36
α	0.97
γ	-2.28
θ	3.09

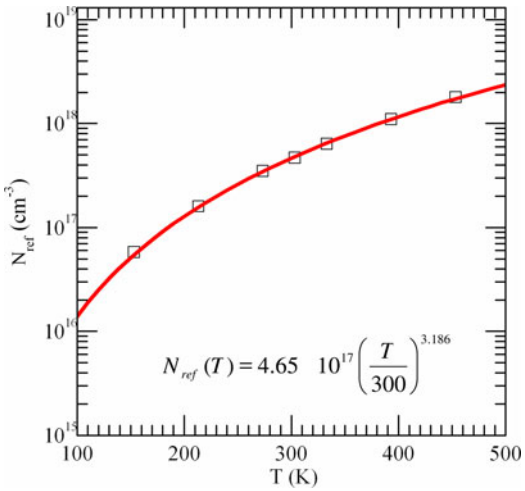

Fig. 5. Temperature dependence of the fitting parameter $N_{\rm ref}$ .This parameter is extracted from the experimental data and subsequently fitted using (5).

in Fig. 4, showing an excellent agreement between measured and modeled $\mu_{\rm max}$. Physically, $\mu_{\rm max}$ accounts for the lattice scattering mechanism. The decrease of $\mu_{\rm max}$ with increase of temperature is mainly because of the increase of lattice vibrations at high temperature.

The data for $N_{\rm ref}$ are plotted in a similar fashion in Fig. 5. Like $\mu_{\rm max}$, the fitting for $N_{\rm ref}$ can be described by the same temperature dependence relationship

$$N_{\rm ref}(T) = N_{\rm ref300K}\left(\frac{T}{300}\right)^{\frac{\theta}{\alpha}} \tag{5}$$

where $N_{\rm ref300\,K}$ is the total reference carrier concentration at 300 K that takes the dopant impurity and carrier–carrier scattering into consideration and affects the mobility sum mainly in the range of $N_A^- + N_D^+ + \Delta n$ that is comparable to it. θ is the power factor to fit the $N_{\rm ref}$ curve and α is from (2). The values obtained are $N_{\rm ref300\,K} = 4.65 \times 10^{17}$ cm^{-3} and $\theta = 3.09$. The resulting fit is plotted in Fig. 5, which shows again an excellent agreement between measured and modeled $N_{\rm ref}$. $N_{\rm ref}$ increases with increasing temperature because at high temperature, lattice scattering becomes dominant compared with impurity and carrier–carrier scattering.

Once we have obtained the temperature dependence of both $N_{\rm ref}$ and $\mu_{\rm max}$, we insert them into (2) to have the complete form of the empirical mobility model in terms of temperature,

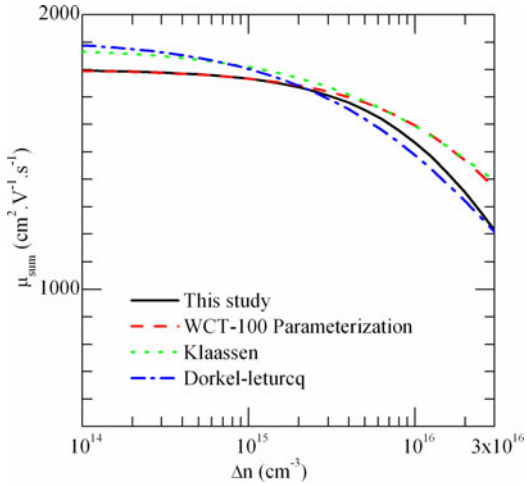

Fig. 6. Comparison of the empirical mobility sum from this study with the existing mobility models from WCT-100 parameterization, Klaassen and Dorkel–Leturcq as a function of injection at 300 K at a doping density of 4×10^{13} cm^{-3}.

ionized dopant density, and carrier injection level:

$$\mu_{\rm sum} = \mu_{\rm max\,300K}\left(\frac{T}{300}\right)^{\gamma} + \frac{\left(\mu_{\rm min\,300K} - \mu_{\rm max\,300K}\right)\left(\frac{T}{300}\right)^{\gamma}}{1 + \left(\frac{1}{\beta}\right)\left(\frac{N_{\rm ref300K}}{N_A^- + N_D^+ + \Delta n}\right)^{\alpha}\left(\frac{T}{300}\right)^{\theta}} \tag{6}$$

where $\mu_{\rm min300\,K} = \mu_{\rm max300\,K}/\beta$, the parameters in (6) are summarized in Table I.

V. COMPARISON TO OTHER MODELS

A. Applicability as a Function of Carrier Injection

In this section, the empirical model is compared with other mobility models in order to assess its validity. First, a comparison is made as a function of carrier injection level. Fig. 6 shows the resulting mobility sum from this study and the mobility models from WCT-100 parameterization, Klaassen [26]–[28], and Dorkel–Leturcq [29] with a doping density of 4×10^{13} cm^{-3} (100-Ω.cm sample) at 300 K in the 1×10^{14} to 3×10^{16} cm^{-3} carrier injection range. The empirical model derived here from the photoconductance measurements is in good agreement with the existing injection dependence mobility models, especially in the range of injection levels relevant for the characterization of silicon wafers by photoconductance measurements, that is, from approximately 1×10^{15} to 3×10^{16} cm^{-3}. In this range, (6) gives intermediate values to the other models. For injection levels below 1×10^{15} cm^{-3}, (6) coincides with WCT-100 parameterization, but is about 10% lower than the Klaassen and Dorkel–Leturcq models. Equation (6) predicts a lower mobility sum than Klaassen's and WCT-100 parameterization beyond an injection level of 1×10^{15} cm^{-3}, but it is close to the model of Dorkel–Leturcq up to an injection level of 3×10^{16} cm^{-3}.

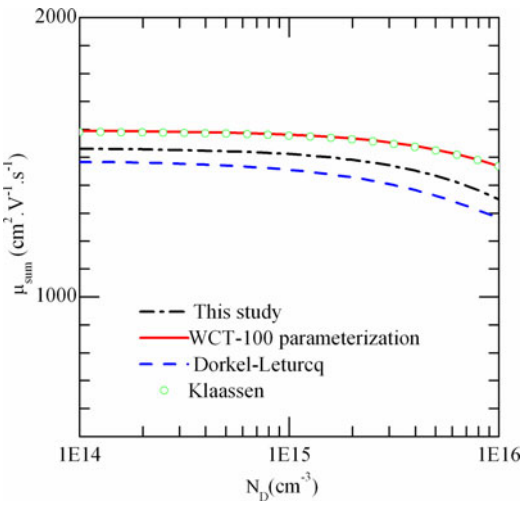

Fig. 7. Comparison of the empirical mobility sum from this study with the existing mobility models from WCT-100 parameterization, Klaassen and Dorkel–Leturcq as a function of doping density at 300 K and injection level of 1×10^{16} cm^{-3}.

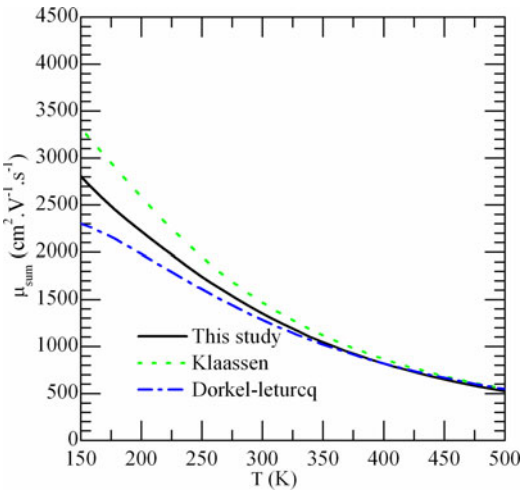

Fig. 8. Comparison of the empirical mobility sum from this study with the existing mobility models from Klaassen and Dorkel–Leturcq as a function of temperature at doping density of 1×10^{16} cm^{-3} and injection level of 1×10^{16} cm^{-3}.

B. Modeling the Influence of Dopant Density

Fig. 7 shows the doping dependence of the mobility sum computed at 300 K and at an injection level of 1×10^{16} cm^{-3}. The mobility models from Klaassen, Dorkel–Leturcq, and WCT-100 parameterization are included for comparison. The mobility predicted from our empirical model lies within the mobilities from other the models and is in reasonable agreement with them, even if it is slightly lower at high dopant concentrations. The most heavily doped sample used in this experiment is $N_D = 1 \times 10^{16}$ cm^{-3}. Therefore, the empirical model of (6) may not be valid for samples doped more than 1×10^{16} cm^{-3}.

C. Modeling the Influence of Temperature

Fig. 8 shows the modeled temperature dependence of the mobility sum from the empirical model together with the mobility models from Klaassen and Dorkel–Leturcq. WCT-100 parameterization is not included as it does not include temperature dependence. The mobility sum is computed at a doping density of 1×10^{16} cm^{-3} and an injection level of 1×10^{16} cm^{-3}. The empirical model is in good agreement with both Klaassen's and Dorkel–Leturcq's models especially at high temperatures. The empirical model may not be valid at temperatures below 150 K.

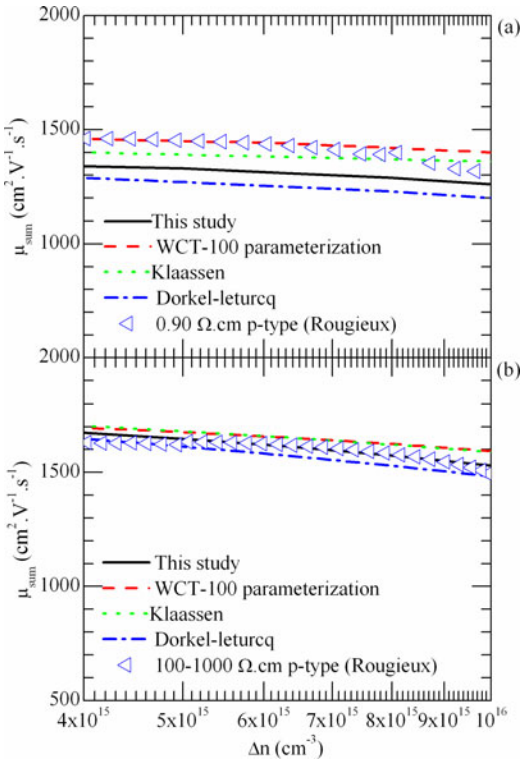

Fig. 9. Comparison of the empirical mobility sum from this study with the existing mobility models from WCT-100 parameterization, Klaassen and Dorkel-Leturcq, and data measured by Rougieux as a function of injection at 300 K for 0.9 Ω·cm and 100–1000 Ω·cm p-type boron doped silicon.

D. Modeling p-type Silicon

The empirical expression derived in this paper is only based on mobility sums measured in *n*-type silicon and the comparisons with other models in the previous sections are based on *n*-type silicon. In this section, the empirical expression is compared with mobility sum data at 300 K previously measured by the photoconductance technique on p-type boron doped 0.9 Ω.cm and 100–1000-Ω.cm silicon [13]. Fig. 9 shows the mobility sum data for a 0.9 Ω.cm p-type sample [see Fig. 9(a)] and a 100–1000-Ω.cm sample [see Fig. 9(b)]. The mobility models from WCT-100 parameterization, Klaassen and Dorkel–Leturcq are also included for comparison. With less than 10% deviation from the experimental data in the injection range displayed, the empirical model is therefore also applicable to p-type boron doped samples of resistivity ranging from 0.9 to 100-Ω.cm samples in injection level spanning from 4×10^{15} to 1×10^{16} cm^{-3} at 300 K. The model may be less accurate for other resistivity samples and conditions outside this injection level and temperature range.

VI. Conclusion

In this paper, we have established a simple empirically based mobility sum model as a function of doping density, injection level, and temperature, based on contactless photoconductance measurements of *n*-type phosphorus doped silicon samples. The empirical model derived here predicts stronger injection dependence at high injection level, and stronger doping dependence at high dopant concentration than Klaassen's, Dorkel–Leturcq's, and the WCT-100 parameterization. For *n*-type phosphorus doped silicon, the empirical model is most accurate within a carrier injection range of 3×10^{15} to 3×10^{16} cm^{-3}, doping density from 4×10^{15} (100 Ω·cm) to 1×10^{16} cm^{-3} (0.5 Ω.cm) and temperature from 150 K to 450 K. The model may not be as accurate outside these ranges. We have verified that the model is also valid for p-type silicon at 300 K. Beyond applications for lifetime spectroscopy measurements, the experimental results presented here also validate the use of Klaassen's model to calculate the carrier diffusion length and the resistivity in moderately injected bulk regions of high efficiency silicon solar cells [30].

References

[1] S. Rein, T. Rehrl, W. Warta, and S. W. Glunz, "Lifetime spectroscopy for defect characterization: Systematic analysis of the possibilities and restrictions," *J. Appl. Phys.*, vol. 91, pp. 2059–2070, 2002.

[2] B. B. Paudyal, K. R. McIntosh, D. H. Macdonald, B. S. Richards, and R. A. Sinton, "The implementation of temperature control to an inductive-coil photoconductance instrument for the range of 0–230 °C," *Prog. Photovoltaics: Res. Appl.*, vol. 16, pp. 609–613, 2008.

[3] J. C. Irvin, "Resistivity of bulk silicon and of diffused layers in silicon," *Bell Syst. Tech. J.*, vol. 41, pp. 387–410, 1962.

[4] P. W. Chapman, O. N. Tufte, J. D. Zook, and D. Long, "Electrical properties of heavily doped silicon," *J. Appl. Phys.*, vol. 34, pp. 3291–3295, 1963.

[5] M. Finetti and A. M. Mazzone, "Impurity effects on conduction in heavily doped n-type silicon," *J. Appl. Phys.*, vol. 48, pp. 4597–4600, 1977.

[6] W. R. Thurber, R. L. Mattis, Y. M. Liu, and J. J. Filliben, "*The Relationship Between Resistivity and Dopant Density for phosphorus- and Boron-doped Silicon,"* Washington, DC, USA:U.S. Dept. Commerce, Nat. Bureau Std. Special Pub., pp. 400–464, 1981.

[7] E. Fourmond, M. Forster, R. Einhaus, H. Lauvray, J. Kraiem, and M. Lemiti, "Electrical properties of boron, phosphorus and gallium co-doped silicon," *Energy Procedia*, vol. 8, pp. 349–354, 2011.

[8] F. Schindler, M. C. Schubert, A. Kimmerle, J. Broisch, S. Rein, W. Kwapil, and W. Warta, "Modeling majority carrier mobility in compensated crystalline silicon for solar cells," *Sol. Energy Mater. Sol. Cells*, vol. 106, pp. 31–36, 2012.

[9] F. Dannhäuser, "Die abhängigkeit der trägerbeweglichkeit in silizium von der konzentration der freien ladungsträger—I," *Solid-State Electron.*, vol. 15, pp. 1371–1375, 1972.

[10] J. Krausse, "Die abhängigkeit der trägerbeweglichkeit in silizium von der konzentration der freien ladungsträger—II," *Solid-State Electron.*, vol. 15, pp. 1377–1381, 1972.

[11] D. H. Neuhaus, P. P. Altermatt, R. A. B. Sproul, A. Sinton, A. Schenk, A. Wang, and A. G. Aberle, "Method for measuring majority and minority carrier mobility in solar cells," in *Proc. 17th Eur. Photovoltaic Sol. Energy Conf.*, 2001, pp. 242–245.

[12] Z. Hameiri, T. Trupke, and R. Sinton, "Determination of carrier mobility sum in silicon wafers by combined photoluminescence and photoconductance measurements," in *Proc. 27th Eur. Photovoltaic Sol. Energy Conf. Exhib.*, 2012, pp. 1477–1481.

[13] F. E. Rougieux, Z. Peiting, M. Thiboust, J. Tan, N. E. Grant, D. H. Macdonald, and A. Cuevas, "A contactless method for determining the carrier mobility sum in silicon wafers," *IEEE J. Photovoltaics*, vol. 2, pp. 41–46, Jan. 2012.

[14] A. Richter, S. W. Glunz, F. Werner, J. Schmidt, and A. Cuevas, "Improved quantitative description of auger recombination in crystalline silicon," *Phys. Rev. B*, vol. 86, p. 165202, 2012.

[15] A. Cuevas, "Modelling silicon characterisation," *Energy Procedia*, vol. 8, pp. 94–99, 2011.

[16] J. Tan, D. Macdonald, F. Rougieux, and A. Cuevas, "Accurate measurement of the formation rate of iron–boron pairs in silicon," *Semicond. Sci. Technol.*, vol. 26, p. 055019, 2011.

[17] P. P. Altermatt, J. Schmidt, M. Kerr, G. Heiser, and A. G. Aberle, "Exciton-enhanced auger recombination in crystalline silicon under intermediate and high injection conditions," in *Proc. 16th Eur. Photovoltaics Sol. Energy Conf.*, 2000, pp. 243–246.

[18] K. R. McIntosh and R. A. Sinton, "Uncertainty in photoconductance lifetime measurements that use an inductive-coil detector," in *Proc. 23rd Eur. Photovoltaic Sol. Energy Conf.*, Valencia, Spain, 2008, pp. 77–82.

[19] P. P. Altermatt, A. Schenk, and G. Heiser, "A simulation model for the density of states and for incomplete ionization in crystalline silicon. I. Establishing the model in Si:P," *J. Appl. Phys.*, vol. 100, p. 113714, 2006.

[20] P. P. Altermatt, A. Schenk, B. Schmithusen, and G. Heiser, "A simulation model for the density of states and for incomplete ionization in crystalline silicon. II. Investigation of Si:As and Si:B and usage in device simulation," *J. Appl. Phys.*, vol. 100, pp. 113715–113717, 2006.

[21] F. J. Blatt, "Scattering of carriers by ionized impurities in semiconductors," *J. Phys. Chemistry Solids*, vol. 1, pp. 262–269, 1957.

[22] H. S. Bennett, "Hole and electron mobilities in heavily doped silicon: Comparison of theory and experiment," *Solid-State Electron.*, vol. 26, pp. 1157–1166, 1983.

[23] N. D. Arora, J. R. Hauser, and D. J. Roulston, "Electron and hole mobilities in silicon as a function of concentration and temperature," *IEEE Trans. Electron Devices*, vol. 29, pp. 292–295, 1982.

[24] G. W. Ludwig and R. L. Watters, "Drift and conductivity mobility in silicon," *Phys. Rev.*, vol. 101, pp. 1699–1701, 1956.

[25] F. J. Morin and J. P. Maita, "Electrical properties of silicon containing arsenic and boron," *Phys. Rev.*, vol. 96, pp. 28–35, 1954.

[26] D. B. M. Klaassen, "A unified mobility model for device simulation," in *Proc. Int. Electron Devices Meet., Tech. Digest.*, 1990, pp. 357–360.

[27] D. B. M. Klaassen, "A unified mobility model for device simulation—I. Model equations and concentration dependence," *Solid-State Electron.*, vol. 35, pp. 953–959, 1992.

[28] D. B. M. Klaassen, "A unified mobility model for device simulation—II. Temperature dependence of carrier mobility and lifetime," *Solid-State Electron.*, vol. 35, pp. 961–967, 1992.

[29] J. M. Dorkel and P. Leturcq, "Carrier mobilities in silicon semi-empirically related to temperature, doping and injection level," *Solid-State Electron.*, vol. 24, pp. 821–825, 1981.

[30] P. J. Cousins, D. D. Smith, L. Hsin-Chiao, J. Manning, T. D. Dennis, A. Waldhauer, K. E. Wilson, G. Harley, and W. P. Mulligan, "Generation 3: Improved performance at lower cost," in *Proc. 35th IEEE Photovoltaic Spec. Conf.*, 2010, pp. 000275–000278.

Authors' photographs and biographies not available at the time of publication.